Human Molecular Genetics, 2014, Vol. 23, No. 14 **3706–3715**
doi:10.1093/hmg/ddu079
Advance Access published on February 20, 2014

Enhanced Ca^{2+} influx from STIM1–Orai1 induces muscle pathology in mouse models of muscular dystrophy

Sanjeewa A. Goonasekera[1,†], Jennifer Davis[1,†], Jennifer Q. Kwong[1], Federica Accornero[1], Lan Wei-LaPierre[3], Michelle A. Sargent[1], Robert T. Dirksen[3] and Jeffery D. Molkentin[1,2,*]

[1]Department of Pediatrics, University of Cincinnati and [2]Howard Hughes Medical Institute, Cincinnati Children's Hospital Medical Center, Cincinnati, OH, USA and [3]Department of Pharmacology and Physiology, University of Rochester Medical Center, Rochester, NY, USA

Received November 14, 2013; Revised January 29, 2014; Accepted February 17, 2014

Muscular dystrophy is a progressive muscle wasting disease that is thought to be initiated by unregulated Ca^{2+} influx into myofibers leading to their death. Store-operated Ca^{2+} entry (SOCE) through sarcolemmal Ca^{2+} selective Orai1 channels in complex with STIM1 in the sarcoplasmic reticulum is one such potential disease mechanism for pathologic Ca^{2+} entry. Here, we generated a mouse model of STIM1 overexpression in skeletal muscle to determine whether this type of Ca^{2+} entry could induce muscular dystrophy. Myofibers from muscle-specific STIM1 transgenic mice showed a significant increase in SOCE in skeletal muscle, modeling an observed increase in the same current in dystrophic myofibers. Histological and biochemical analysis of STIM1 transgenic mice showed fulminant muscle disease characterized by myofiber necrosis, swollen mitochondria, infiltration of inflammatory cells, enhanced interstitial fibrosis and elevated serum creatine kinase levels. This dystrophic-like disease in STIM1 transgenic mice was abrogated by crossing in a transgene expressing a dominant-negative Orai1 (dnOrai1) mutant. The dnOrai1 transgene also significantly reduced the severity of muscular dystrophy in both *mdx* (dystrophin mutant mice) and δ-sarcoglycan-deficient (*Sgcd*$^{-/-}$) mouse models of disease. Hence, Ca^{2+} influx across an unstable sarcolemma due to increased activity of a STIM1–Orai1 complex is a disease determinant in muscular dystrophy, and hence, SOCE represents a potential therapeutic target.

INTRODUCTION

Muscular dystrophy encompasses both a clinically and genetically heterogeneous group of disorders that result in progressive muscle weakness due to degeneration of skeletal muscle (1). Although the majority of genes responsible for muscular dystrophy are associated with maintaining sarcolemmal integrity and linking the cytoskeleton to the extracellular matrix, the exact cause for myofiber degeneration is uncertain (1,2). Numerous reports have suggested that the loss of Ca^{2+} homeostasis contributes to the development of the dystrophic phenotype and overt myofiber necrosis (3–9). Specifically, the imbalance between sarcolemmal Ca^{2+} influx and efflux pathways in dystrophic myofibers is hypothesized to elevate Ca^{2+} levels sufficient to result in mitochondrial Ca^{2+} overload, endoplasmic reticulum stress, increased oxidative stress and activation of Ca^{2+}dependent proteases triggering multiple necrotic and apoptotic pathways (4,6,9–11). Currently, there is no cure for muscular dystrophy; hence identifying the molecular mechanisms that promote myofiber Ca^{2+} overload could suggest new therapeutic targets.

One such Ca^{2+} influx pathway that might contribute to enhanced cytosolic Ca^{2+} entry in dystrophic muscle is store-operated Ca^{2+} entry (SOCE) (3,12,13). Indeed, skeletal muscle expresses STIM1 and Orai1 in abundance, which serves as the main channel constituents mediating SOCE in skeletal muscle (13–18). While SOCE can reload sarcoplasmic reticulum (SR) Ca^{2+} levels, the true physiological relevance of SOCE in skeletal muscle remains controversial (14,19–22). Genetic mouse models with deletion of *Stim1* and *Orai1* showed impaired skeletal muscle growth and perinatal lethality,

*To whom correspondence should be addressed at: Cincinnati Children's Hospital Medical Center, Cincinnati, 240 Albert Sabin Way, MLC7020, Cincinnati, OH 45229, USA. Email: jeff.molkentin@cchmc.org
†These authors contributed equally to this study.

suggesting that this channel complex does have a physiologic role in skeletal muscle (21,23,24). STIM1 has also been shown to reload SR Ca^{2+} stores through its interaction with Orai and transient receptor potential canonical (TRPC) channels (25). How STIM1 and Orai interact to enhance SOCE has not been fully elucidated, but a recent study suggests that Orai activity is graded by the number of associated STIM1 molecules (26). Muscle-specific expression of dominant negative Orai1 (dnOrai1) results in viable adult mice that exhibit reduced skeletal muscle growth and increased fatigability (27).

Recent reports have also suggested that increases in SOCE are associated with muscular dystrophy, although these studies did not specifically address the mechanistic involvement of STIM1 or Orai1 in contributing to disease (3,13,18,28). STIM1 and Orai1 are considered to be both necessary and sufficient for SOCE in many tissues; however, involvement of TRP channel family members might also contribute to some forms of SOCE (3,28–34). Here, we show for the first time that enhanced muscle-specific expression of STIM1 protein and a concomitant increase in sarcolemmal Ca^{2+} influx gives rise to histological and biochemical features of muscular dystrophy. More importantly, many of these pathological features are mitigated by skeletal muscle-specific expression of dominant negative Orai1 (dnOrai1), which is sufficient to block increased SOCE that typifies dystrophic myofibers.

RESULTS

Generation and characterization of muscle-specific STIM1 transgenic mice

As shown previously (3,13,18), myofibers from dystrophic mice have induced and significantly elevated SOCE-like activity (Supplementary Material, Fig. S1A and B). To address the potential functional effects associated with increased SOCE in dystrophic myofibers, we generated a mouse model of STIM1 overexpression in skeletal muscle using the human skeletal α-actin promoter. Three transgenic founder lines were obtained and one of the two lower expressing lines was selected for further analysis, although key results were confirmed in at least one other line (Fig. 1A). STIM1 was expressed ∼6-fold higher in the transgenic (TG) quadriceps compared with wild-type (Wt) (Fig. 1B). STIM1 was uniformly expressed across a broad range of skeletal muscle groups in Wt and at much higher levels in STIM1 TG mice, although almost no expression was observed in the heart (Fig. 1C). STIM1 immunofluorescent staining of quadriceps muscle cross-sections also demonstrated the distribution and level of expression of the STIM1 transgene (Fig. 1D). Immunocytochemical analysis of isolated myofibers showed that STIM1 protein largely co-localized with the ryanodine receptor 1 (RyR1) in the SR as previously demonstrated (Fig. 1E) (23). Interestingly, overexpression of STIM1 in skeletal muscle mildly enhanced the protein levels of Orai1 and STIM2, likely by generating a larger or more stable complex in the membrane (Fig. 1F).

Photometry experiments to assess SOCE in flexor digitorum brevis (fdb) fibers showed a 2-fold increase in Ca^{2+} influx from STIM1 TG mice compared with controls (Fig. 1G and H). For these experiments, SR store depletion was achieved by pre-treatment with cyclopiazonic acid (CPA, SERCA1 inhibitor) in Ca^{2+} free external media, followed by acute Ca^{2+} addition in the buffer to induce SOCE current. Interestingly, Ca^{2+} ratios were found to be significantly elevated in fibers from STIM1 TG compared with Wt mice (Fig. 1I), but no differences were observed in the amplitude of electrically evoked Ca^{2+} transients, decay time and the RyR releasable SR Ca^{2+} pool measured in response to a 4-chloro-m-cresol (4-cmc) bolus, which maximally activates the RyR (Supplementary Material, Fig. S1C–F).

STIM1 overexpression produces classic features of muscular dystrophy

Histological analysis of H&E and Masson's trichrome-stained sections from diaphragm, quadriceps and soleus revealed extensive pathology with increased incidence of myofibers with centrally localized nuclei at 6 weeks and 6 months of age in STIM1 TG mice compared with Wt mice (Fig. 2A and B), as well as infiltration of inflammatory cells, fiber size irregularities and enhanced interstitial fibrosis (Fig. 2A and C). Hydroxyproline content, another measure of tissue fibrosis, was also increased in muscles from STIM1 TG mice (Fig. 2D). Serum creatine kinase (CK) levels were also elevated in STIM1 TG mice at 6 weeks and 6 months compared with Wt mice (Fig. 2E). Moreover, calpain enzymatic activity, as measured in the absence of exogenous Ca^{2+} by a Calpain Glo Assay (see Materials and Methods), was significantly elevated in STIM1 TG muscle lysates compared with Wt muscle, consistent with the elevated cytosolic Ca^{2+} profile presented earlier (Fig. 2F). Enhanced basal Ca^{2+} levels can also activate the Ca^{2+}dependent phosphatase calcineurin leading to increased activity of nuclear factor of activated T-cells (NFAT), which was markedly increased in STIM1 TG skeletal muscle (Fig. 2G). Hence, the increased SOCE and cytosolic Ca^{2+} levels in skeletal muscle of STIM1 TG mice promoted pathology reminiscent of that observed in muscular dystrophy.

STIM1 overexpression leads to mitochondrial pathology

Elevated cytosolic Ca^{2+} is known to negatively impact mitochondrial morphology and function, as well as increase necrotic cell death of myofibers due to mitochondrial rupture (35). Using transmission electron microscopy, we observed that mitochondria from STIM1 TG muscle appeared fragmented, swollen and/or ruptured compared with Wt controls (Fig. 3A). Enhanced Ca^{2+} uptake into mitochondria can result in mitochondrial swelling leading to the opening of the permeability transition pore (11,36). Indeed, mitochondria isolated from STIM1 TG mice demonstrated a lower capacity to swell in response to a Ca^{2+} bolus but a greater ability to shrink compared with mitochondria isolated from Wt mice, demonstrating that they are already partially swollen (Fig. 3B and C). Mitochondria isolated from STIM1 TG muscle showed a 2-fold increase in matrix Ca^{2+} compared with Wt mitochondria (Fig. 3D). Interestingly, baseline oxygen consumption was also significantly elevated in STIM1 mitochondria compared with Wt, which is consistent with elevated mitochondrial matrix Ca^{2+} levels (Fig. 3E). However, no changes in select electron transport chain inner mitochondrial proteins or the outer mitochondrial transporter voltage-dependent anion channel (VDAC) were observed in muscle from STIM1 TG mice (Fig. 3F). Thus, enhanced STIM1 activity leads to elevated

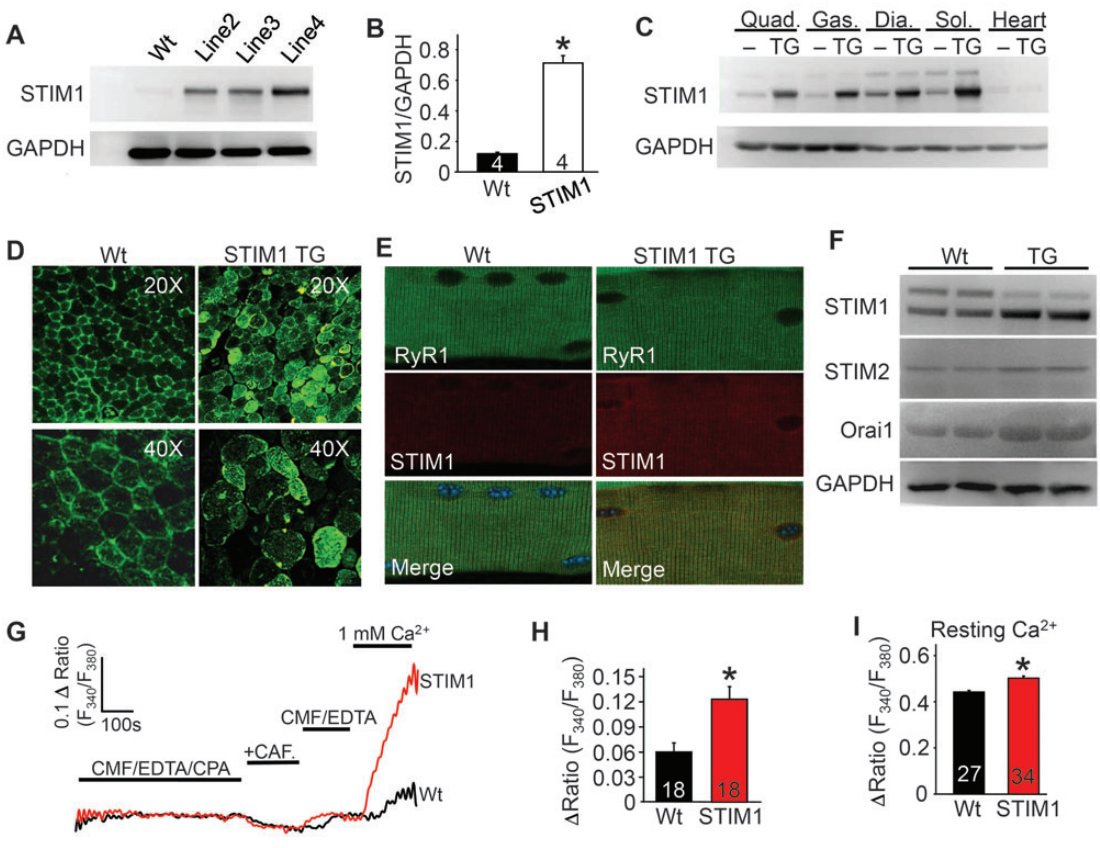

Figure 1. Generation of STIM1 overexpressing TG mice. (**A**) Western blot analysis of STIM1 expression in the quadriceps of Wt and three different STIM1 TG founder lines. (**B**) Western blot quantification of STIM1 protein overexpression levels in line 2. $^*P < 0.05$ compared with Wt mice and number of animals analyzed is shown in the bars. (**C**) Western blot analysis of STIM1 expression in different muscles and heart in Wt and STIM1 TG mice of line 2 (abbreviations: Quad, quadriceps; Gas, gastrocnemius; Dia, diaphragm; Sol, soleus). (**D**) Immunofluorescence analysis of STIM1 expression (green) in 10 μm sections of quadriceps muscle from Wt and STIM1 TG mice. (**E**) Immunohistochemical analysis of STIM1 localization (red) versus ryanodine receptor (green) in fdb myofibers isolated from Wt and STIM1 TG mice. The merge shows co-expression of both as yellow. (**F**) Representative western blots of STIM1, STIM2 and Orai1 expression in skeletal muscle from Wt and STIM1 TG mice. (**G**) Representative traces of sarcolemmal Ca^{2+} entry assessed following SR store depletion then immediate repletion of Ca^{2+} in Wt (*black*) and STIM1 TG (*red*) fdb fibers. CAF, caffeine; CMF, Ca^{2+} and Mg^{2+} free Ringers; CPA, cyclopiazonic acid. (**H**) Average maximal peak amplitude of Ca^{2+} influx in Wt and STIM1 TG fdb myofibers at 1 mM external Ca^{2+} in experiments shown in "G". (**I**) Analysis of resting Ca^{2+} levels in ratiometric photometry experiments carried out in Wt and STIM1 TG fdb fibers. $^*P < 0.05$ compared with Wt mice and number of fdb fibers analyzed per condition is shown in the bars of each panel.

Ca^{2+} that causes greater mitochondrial Ca^{2+} loading, swelling and rupture, secondarily facilitating myofiber necrosis.

Rescue of muscle pathology in STIM1 TG mice by coexpression of dnOrai1

To determine whether the muscular dystrophy-like disease observed in STIM1 TG mice was specifically mediated by enhanced SOCE through STIM1–Orai1 channel complexes, we crossed STIM1 TG mice with a skeletal muscle-specific mouse model expressing dnOrai1 (27,37). To ensure that both transgenes were expressed at comparable levels in the double transgenic (DTG) state, western blotting was performed for STIM1, and anti-hemagglutinin (HA) antibody was used to detect the dnOrai1 protein (27). The results showed no reduction in STIM1 or HA signal in skeletal muscle from double transgenic (DTG) versus single TG mice (Fig. 4A). Previously, dnOrai1 mice were shown to be viable and fertile, although they exhibited reduced skeletal muscle growth and increased fatigability (27). However, this increase in fatigability was not of concern because we observed that the overwhelming effect of the dnOrai1 transgene was to silence SOCE entry and underlying muscle pathology when crossed with dystrophic mouse models. For example, the muscular dystrophy-like disease in STIM1 TG transgenic mice was significantly attenuated by the dnOrai1 transgene, including a reduction in myofibers with centrally localized nuclei, reduced serum CK, less fiber irregularities and immune infiltrates and a trend toward reduced interstitial fibrosis (Fig. 4B–E). The dnOrai1 protein functioned as expected in that SOCE produced by STIM1 overexpression was essentially abolished, and calpain activity was significantly reduced (Fig. 4F and G). These results indicate that the dnOrai1 transgene directly antagonized the disease causing effects of STIM1 overexpression in skeletal muscle, further confirming that the STIM1–Orai1 channel complex comprises the primary molecular mechanism of SOCE in this tissue.

DnOrai1 expression mitigates the dystrophic phenotype in *mdx* and *Sgcd*$^{-/-}$ mice

To address whether STIM1 is upregulated in mouse models of muscular dystrophy, we assessed STIM1 protein expression in

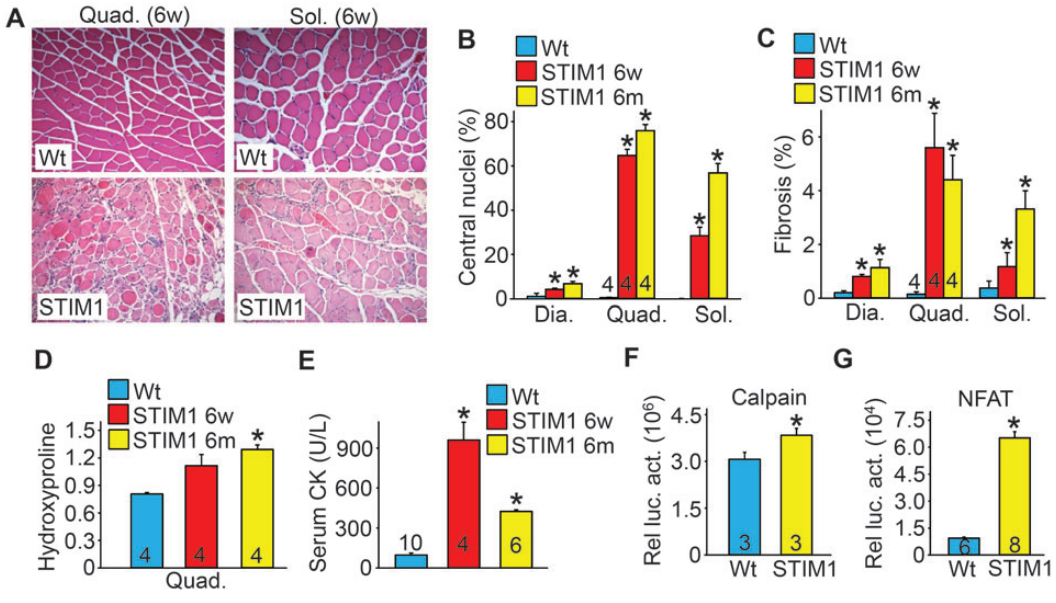

Figure 2. STIM1 overexpression in skeletal muscle gives rise to histological and biochemical features of muscular dystrophy. (**A**) Representative H&E-stained histological sections from quadriceps and soleus muscle obtained from 6-week-old Wt and STIM1 TG mice. Magnification is ×200. (**B**) Quantification of myofibers with centrally located nuclei as a maker of regeneration in the diaphragm (three sections/muscle were analyzed), quadriceps (five sections/muscle were analyzed) and soleus (two sections/muscle were analyzed) muscles in Wt and STIM1 TG mice at 6 weeks and 6 months. The total number of mice/muscles analyzed is shown in the bars for the quadriceps. (**C**) Interstitial fibrosis quantified by metamorph analysis software in Masson's trichrome-stained histological sections of diaphragm (Dia), quadriceps (Quad) and soleus (Sol) obtained from mice sacrificed at the indicated ages. (**D**) Biochemical analysis of hydroxyproline content for fibrosis in the quadriceps normalized to muscle weight in Wt and STIM1 TG mice. (**E**) Quantitation of serum creatine kinase (CK) levels in Wt and STIM1 TG mice at 6 weeks and 6 months. (**F**) Quantitation of calpain activity in Wt and STIM1 TG quadriceps at 6 weeks of age (Relative luciferase activity is shown as part of a calpain assay). (**G**) NFAT luciferase activity assessed in muscle lysates obtained from Wt and STIM1 TG mice also carrying the NFAT luciferase reporter transgene. $^{*}P < 0.05$ compared with Wt mice and the number of animals used as shown in the bars of each panel.

the quadriceps of 3-month-old *mdx* and *Sgcd*$^{-/-}$ dystrophic mice, which indeed showed a significant upregulation of STIM1 protein, although it was primarily the spliced form generating the smaller isoform of STIM1 (Fig. 5A and B, see Materials and Methods for description of spliced forms of STIM1 used to make the TG mice). To specifically assess if STIM1/Orai1-mediated Ca^{2+} influx contributes to the development of muscular dystrophy *in vivo*, we crossed dnOrai1 TG mice with the *mdx* and *Sgcd*$^{-/-}$ dystrophic mouse models. Expression of dnOrai1 protein in skeletal muscle led to a dramatic improvement in histopathology in *mdx* diaphragm and quadriceps, including significantly reduced central nucleation, fibrosis, inflammatory cell infiltration and areas with necrotic myofibers (Fig. 5C–E). Consistent with these data, compound *mdx* dnOrai1 TG mice showed a significant decrease in serum CK levels compared with *mdx* controls (Fig. 5F). Global muscle performance as assessed by treadmill running was significantly improved in compound *mdx* dnOrai1 TG mice compared with *mdx* controls (Fig. 5G). These results were likely due to decreased Ca^{2+} entry from endogenous SOCE channels, which would normally lead to muscle wasting disease, as the typical increase in this Ca^{2+} entry activity observed in *mdx* myofibers was abolished by expression of the dnOrai1 transgene (Fig. 5H). *In situ* isometric force in compound *mdx* dnOrai1 tibialis anterior (TA) muscle was significantly less when compared with *mdx* mice, which is consistent with the muscle weakness that was previously reported in dnOrai1 muscle (27). However, compound *mdx* dnOrai1 TG muscles (TA) maintained force over a series of five isometric contractions, while *mdx* muscle force production dropped by an average of 40.5 ± 5.8% (Fig. 5J). This ability of the compound *mdx* dnOrai1 mice to retain force likely contributes to their improved running performance despite the lower acute force production.

To extend these results, we also crossed the dnOrai1 TG into the *Sgcd*$^{-/-}$ background, which is a mouse model of limb-girdle muscular dystrophy that shows a more severe disease phenotype compared with *mdx* mice. Similar to our results in *mdx* mice, *Sgcd*$^{-/-}$ mice expressing the dnOrai1 transgene exhibited reduced central nucleation (Fig. 5K), decreased serum CK levels (Fig. 5L) and increased tolerance to treadmill running (Fig. 5M). As was observed in *mdx* myofibers, enhanced Ca^{2+} influx was nearly abolished in fibers from compound *Sgcd*$^{-/-}$ dnOrai1 TG mice compared with *Sgcd*$^{-/-}$ controls (Fig. 5N). Thus, Orai1-dependent SOCE activity serves as an endogenous pathway for pathologic Ca^{2+} entry in at least two mouse models of muscular dystrophy.

DISCUSSION

A commonality among many of the identified human mutations that cause muscular dystrophy is that they affect genes directly or indirectly involved in maintaining the structural integrity of the sarcolemma. Alterations in the properties of the sarcolemma are then hypothesized to promote Ca^{2+} influx that initiates the dystrophic phenotype (3,4,6,7). Indeed, a number of key molecules leading to or resulting from a Ca^{2+} imbalance in muscular dystrophy have been validated (5,6,38,39). For example, we

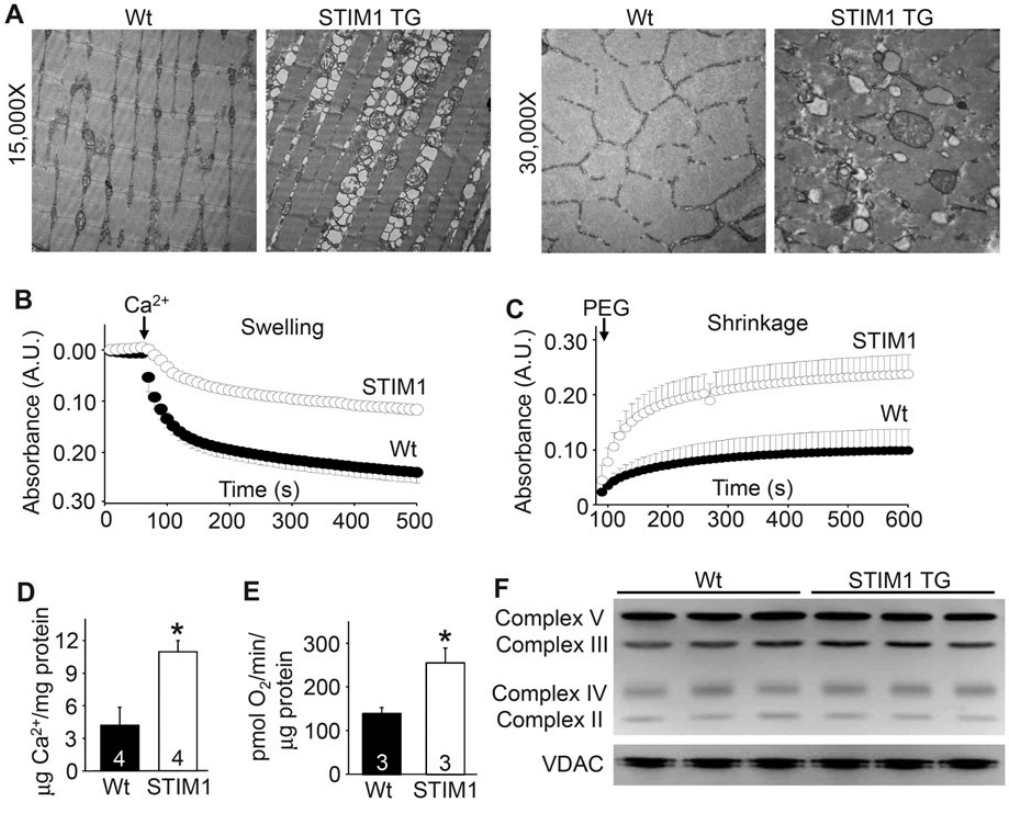

Figure 3. STIM1 overexpression leads to a mitochondrial pathology in muscle. (**A**) Electron microscopic images of Wt and STIM1 TG quadriceps muscle at two different magnifications. (**B**) Light scattering assessed in mitochondria suspension during a Ca^{2+} stimulus to induce swelling derived from Wt (solid) and STIM1 TG (clear) muscle. (**C**) Same assay as in "B" except that mitochondria shrinking was assessed in response to PEG addition. (**D**) Quantitation of mitochondrial matrix Ca^{2+} content in isolated mitochondria from Wt and STIM1 TG muscle. (**E**) Analysis of baseline O_2 consumption in mitochondria isolated from Wt and STIM1 TG muscle. (**F**) Western blot analysis for the indicated mitochondrial proteins in Wt and STIM1 TG muscle protein lysates. $^*P < 0.05$ compared with Wt mice and the number of animals used is shown in each panel in the bars.

demonstrated that overexpression of the sarcoplasmic reticulum Ca^{2+} ATPase-1 (SERCA1) in dystrophic muscle was profoundly protective by promoting more efficient Ca^{2+} reuptake into the SR and lessening Ca^{2+} accumulation in the cytosol (6). Desensitization of the mitochondrial permeability transition pore to calcium overload by deletion of the gene encoding cyclophilin D or by use of a cyclophilin inhibitory drug, reduced Ca^{2+}-mediated mitochondrial swelling, rupture and myofiber necrosis (11,40). Finally, as will be discussed below, we also showed that direct enhancement in Ca^{2+} influx by overexpression of TRPC3 channels in skeletal muscle initiated a dystrophic-like phenotype (3). Here, we show that enhanced Ca^{2+} entry associated with bonafide SOCE activity is a dystrophic disease determinant.

The contribution of Ca^{2+} overload to muscular dystrophy has been previously proposed, although the identity of select Ca^{2+} channels or other mechanisms whereby this ion enters the diseased myofiber remains less certain (3,13,41,42). As discussed above, we showed that TRPC3 overexpression in skeletal muscle gives rise to a dystrophic-like phenotype with enhanced Ca^{2+} entry activity, and that a dominant negative TRPC mutant protein mitigates disease in *Sgcd*$^{-/-}$ mice (3). Similarly, dnTRPV2 overexpression in *mdx* mice reduced muscle pathology, which likely affected the same general membrane complexes associated with TRPC channels (41). TRPC channels were initially proposed to be directly responsible for SOCE, but others have disputed this and suggested that TRPC channels generate an independent current that is not store operated, although it likely influences SOCE mediated by the STIM1–Orai1 complex (43,44).

STIM1–Orai1 coupling was found to be both necessary and sufficient for SOCE current in skeletal myotubes that exhibits the pharmacological and electrophysiological characteristics of Ca^{2+}-release-activated-Ca^{2+} (CRAC) current recorded in T lymphocytes (17). In addition, SOCE in adult skeletal muscle exhibits the physiologic Ca^{2+} entry profile of STIM1–Orai1 channels rather than that generated by TRPC channels, although the involvement of STIM1–Orai1 activity in mediating muscle disease has not been defined (13,18). Hoover and Lewis (26) found that maximal SOCE channel activity is seen when eight STIM molecules are complexed with 1 Orai channel, so overexpression of STIM1 in skeletal muscle could dramatically enhance SOCE through existing Orai channels. However, in our STIM1 overexpressing mice, we also observed a mild increase in Orai1 in skeletal muscle that would support even greater SOCE activity and activation of downstream Ca^{2+}sensitive pathways (mitochondrial swelling, calpain and calcineurin-NFAT). Thus, our collective results add further data to support the hypothesis that enhanced Ca^{2+} influx, leading to greater basal cytosolic Ca^{2+}, directly initiates myofiber death leading to muscular dystrophy.

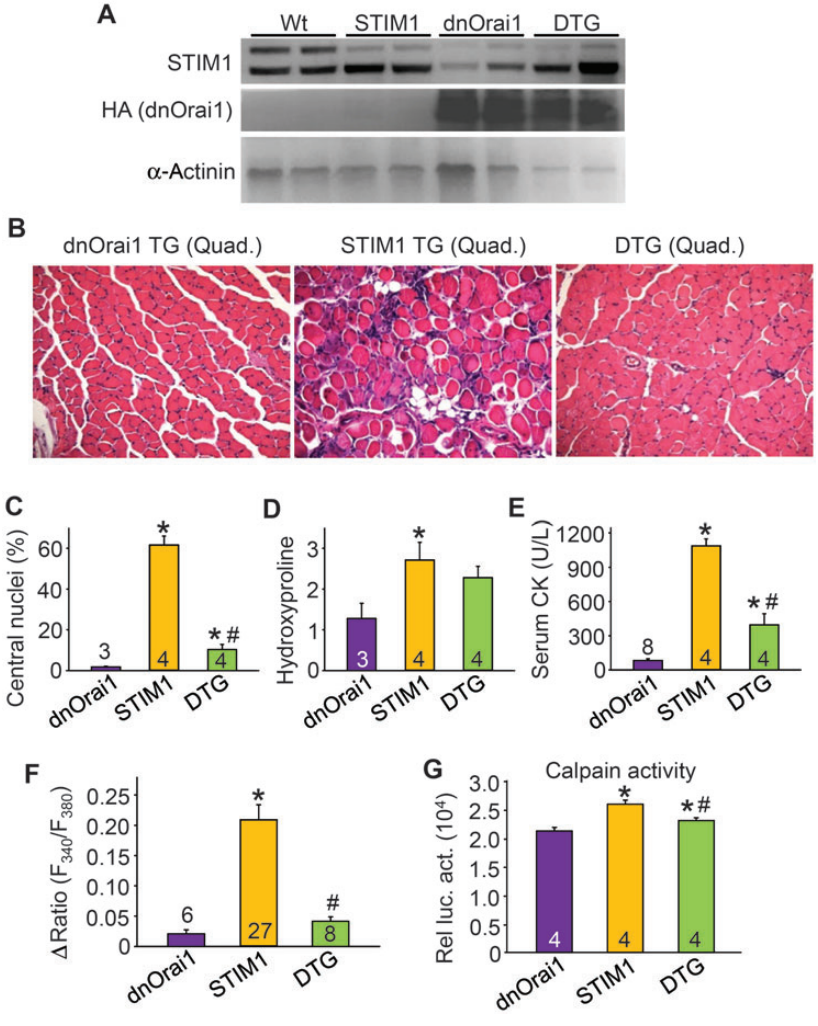

Figure 4. Overexpression of dnOrai1 inhibits STIM1-induced muscle disease. (**A**) Western blot analysis demonstrating the expression of STIM1 and hemagglutinin (HA) tagged dnOrai1 in Wt, STIM1 TG, dnOrai1 TG and DTG quadriceps muscle. α-actinin was used as a loading and sample integrity control. (**B**) H&E-stained histological sections from quadriceps of dnOrai1 TG, STIM1 TG and STIM1/dnOrai1 DTG mice. Magnification is ×200. (**C**) Quantitation of myofibers with centrally located nuclei as a function of regeneration in histological sections of quadriceps (five sections/muscle were analyzed) from the indicated genotypes of mice. (**D**) Quantitation of hydroxylproline content as a measure of interstitial fibrosis in dnOrai1 TG, STIM1 TG and DTG quadriceps. (**E**) Analysis of serum CK levels in the indicated mice. (**F**) Maximal amplitude of Ca^{2+} influx with Ca^{2+} re-addition following SR store depletion in fdb fibers isolated from dnOrai1 TG, STIM1 TG and dnOrai1–STIM1 DTG mice. (**G**) Calpain activity using a luciferase reporter-based assay (relative luciferase activity) in muscle lysates obtained from the indicated genotypes. $^{*}P < 0.05$ compared with dnOrai1 TG, $^{\#}P < 0.05$ compared with STIM1 TG and the number of animals or fdb fibers analyzed is shown in the bars.

Human mutations in the *STIM1* gene have recently been identified (45). These mutations appear to enhance STIM1 protein aggregation in myoblasts in culture and lead to greater Ca^{2+} entry. Individuals with these mutations develop a myopathy that results in lower limb weakness, contractures and elevated serum CK levels (45). At the histological level, muscle biopsies from these patients showed tubular aggregation and fiber size irregularities (45). Thus, while STIM1 transgenic mice and enhanced SOCE lead to muscle pathology with many features of muscular dystrophy, it also could be partially classified as a myopathy, although we did not observe tubular aggregates in our mice (the human mutations in *STIM1* lie within the Ca^{2+} binding EF hands). However, the consistent finding between our mouse model and humans with *STIM1* mutations appears to be that increased SOCE is pathologic and leads to muscle dysfunction and wasting. Finally, the observations in the mouse, such as the ability of dnOrai1 to mitigate muscle pathology in *mdx* and *Sgcd*$^{-/-}$ animals, suggest that agents designed to inhibit Orai1–STIM1 activity might represent a novel therapeutic strategy to reduce pathologic Ca^{2+} influx and myofiber necrosis in muscular dystrophy or myopathy, as well as potentially treating these identified STIM1 mutant patients.

MATERIALS AND METHODS

Ethics statement

All animal procedures and usages were approved by the Institutional Animal Care and Use Committee of the Cincinnati Children's Hospital Medical Center, protocol 2E11104. No human subjects, tissue, or cells were used.

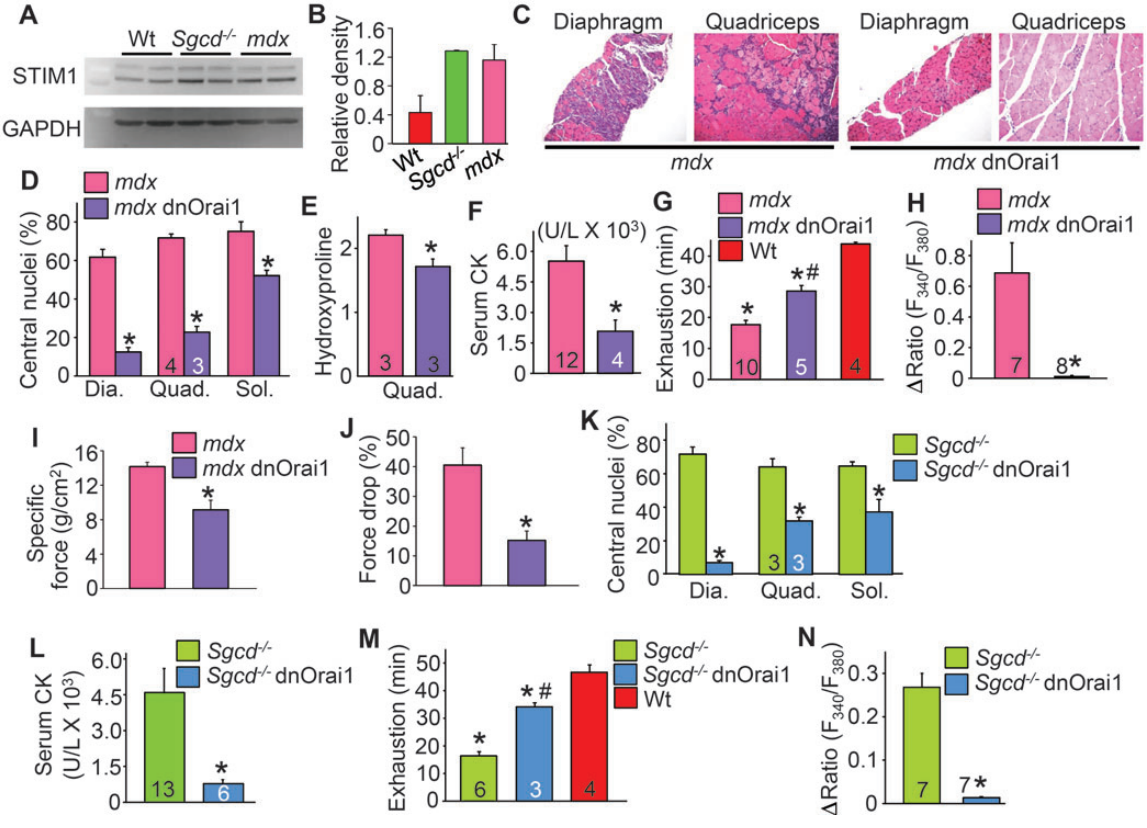

Figure 5. dnOrai1 mitigates muscular dystrophy in two mouse models of this disease. (**A**) Western blot and (**B**) quantification of STIM1 expression from wild-type (Wt), *mdx* and $Sgcd^{-/-}$ quadriceps. A long and short protein isoform of STIM1 can be seen, as previously published (46). (**C**) H&E-stained histological sections of diaphragm and quadriceps from *mdx* and *mdx* dnOrai1 TG mice at 6 weeks of age. Magnification is ×200. (**D**) Quantitation of percentage of myofibers with centrally localized nuclei in the diaphragm (Dia, three sections were analyzed/muscle), quadriceps (Quad, five sections were analyzed/muscle) and soleus (Sol, two sections were analyzed/muscle) of *mdx* and *mdx* dnOrai1 TG mice at 6 weeks of age. (**E**) Hydroxyproline content assessed in the quadriceps muscle of *mdx* and *mdx* dnOrai1 TG as a measure of fibrosis. (**F**) Quantitation of serum CK in *mdx* and *mdx* dnOrai1 TG mice. (**G**) Time to running exhaustion on a treadmill for *mdx*, *mdx* dnOrai1 TG and Wt mice. (**H**) Average maximal amplitude of Ca^{2+} influx following SR store depletion in fdb fibers isolated from *mdx* and *mdx* dnOrai1 TG mice. (**I**) Quantification of the average isometric force produced in *mdx* and *mdx* dnOrai1 TG TA muscle. $^{*}P < 0.05$ compared with *mdx* ($n = 5$). (**J**) Quantification of the loss of isometric force over a series of five isometric contractions. $^{*}P < 0.05$ compared with *mdx* ($n = 5$). (**K**) Quantitation of percentage of myofibers with centrally localized nuclei in the diaphragm, quadriceps and soleus of $Sgcd^{-/-}$ and $Sgcd^{-/-}$ dnOrai1 TG mice at 6 weeks of age. (**L**) Quantitation of serum CK in $Sgcd^{-/-}$ and $Sgcd^{-/-}$ dnOrai1 TG mice. (**M**) Time to running exhaustion on a treadmill in $Sgcd^{-/-}$ and $Sgcd^{-/-}$ dnOrai1 TG mice. (**N**) Amplitude of Ca^{2+} influx following SR store depletion in photometry experiments conducted in acutely isolated fdb fibers from $Sgcd^{-/-}$ and $Sgcd^{-/-}$ dnOrai1 TG mice. $^{*}P < 0.05$ compared with *mdx*/$Sgcd^{-/-}$ mice and the number of animals or fdb fibers analyzed is shown in the bars of each figure panel.

Animals

The human STIM1 cDNA encoding the shorter spliced form (46) was cloned into a modified human skeletal α-actin promoter (47) to create the skeletal muscle-specific TG mice (FVB/N strain). $Sgcd^{-/-}$ mice and line 5 dnOrai1 TG mice with medium expression have been described before (27,48). To generate the STIM-dnOrai1 DTG mice, STIM1 TG mice were mated with C57BL/6 dnOrai1 TG mice and mixed background non-transgenic, single transgenic and DTG littermates were studied from the same litters. To generate the STIM1 TG-*mdx* mice, *mdx* females were mated with male dnOrai1 TG mice, and first-generation males with or without the STIM1 TG were analyzed. To generate the dnOrai1 TG-$Sgcd^{-/-}$ mice, $Sgcd^{-/-}$ females were mated with dnOrai1 TG males and siblings from these litters were subsequently mated, and the third generation was analyzed. Comparisons were always made between littermates with a similar mixed background. NFAT-transgenic reporter mice were previously described (49).

Mitochondrial isolation for swelling/shrinking analysis

Mitochondria were isolated from hind limb muscles of 6-week-old mice as previously described (50). Light scattering was measured using 250 μg of mitochondria suspended in 1 ml of buffer followed by addition of 200 μM $CaCl_2$ or 50% PEG (wt/vol) to induce mitochondrial swelling or shrinking, respectively. Change in absorbance at 540 nm was recorded every 10 s for up to 10 min.

Mitochondrial respiration

Mitochondrial oxygen consumption was measured in isolated muscle mitochondria using an XF24 Analyzer (Seahorse Biosciences). Briefly, mitochondria (2 μg/well) were seeded in XF24 culture plates and respiration was measured in MAS-1 buffer (220 mM mannitol, 70 mM sucrose, 10 mM KH_2PO_4, 5 mM $MgCl_2$, 2 mM HEPES, 1 mM EGTA, 0.2% fatty acid free bovine serum albumin, pH 7.4) supplemented with 10 mM

succinate and 2 μM rotenone. State 3 respiration was initiated with the addition of 4 mM ADP and mitochondrial oxygen consumption was subsequently inhibited with 4 μM antimycin A. The rate of baseline state 3 respiration was determined by subtracting the oxygen consumption in the presence of antimycin A from the rate with ADP.

Analysis of mitochondrial Ca^{2+} content

Muscle mitochondria were isolated and suspended in buffer containing 120 mM KCl, 10 mM Tris pH7.4 and 5 mM KH_2PO_4. Mitochondria were solubilized by freeze thawing followed by sonication and the lysate was subsequently cleared by centrifugation (20 000*g* for 10 min). The Ca^{2+} concentration in the cleared lysate was determined spectrophotometrically using the Calcium Detection Kit (Abcam).

Antibodies

STIM1 was detected using rabbit polyclonal antibody (1:2500, Millipore). Orai1 was detected using a rabbit polyclonal antibody (1:100, Abcam). STIM2 was detected using a rabbit polyclonal antibody (1:300, ProSci). The HA-tagged dnOrai1 construct was detected using an HA mouse monoclonal antibody (1:500, Santa Cruz). Anti-α-actinin mouse monoclonal was used as a control in some experiments (Sigma, 1:500), as was a mouse monoclonal anti-GAPDH antibody (Fitzgerald, 1:10 000). Mitochondrial inner membrane proteins were detected using MitoProfile total OXPHOS rodent western blot antibody cocktail (Abcam). VDAC antibody was also used (Abcam, recognizes VDAC1).

Immunocytochemistry

Muscle fdb fibers were isolated and plated in laminin coated cover slips and fixed with 4% paraformaldehyde for 20 min. Cover slips were rinsed in phosphate buffered saline and blocked with goat serum and NP40%. Attached fibers were incubated with RyR1 (Abcam) and STIM1 (Millipore) antibody overnight and labeled with appropriate secondary antibody the following day. Transmission electron microscopy was used to assess muscle ultrastructure morphology as previously described (51).

Hydroxyproline content analysis and calpain activity

Mice were sacrificed and quadriceps surgically removed and flash frozen. Tissue was then processed for hydroxyproline content quantitation as described previously (52). Tissue calpain activity was measured with the Calpain Glo Assay kit from Promega.

Ca^{2+} measurements

Assessment of Ca^{2+} handling and levels in the fdb myofibers was performed as described previously (3,6). For SOCE experiments, fibers were isolated as above and incubated in CMF Ringers with 30 μM CPA (SERCA inhibitor) and 100 μM EDTA for 45 min. Fibers were rinsed with CMF/CPA/EDTA solution and the Fura 2-AM excitation ratio (340/380 nm) was recorded. Following 3 min of CMF/CPA/EDTA perfusion, the fibers were perfused with 1 or 2 mM Ca^{2+}-containing Ringers for a maximum of 5 min. Baseline to peak Ca^{2+} influx was taken as SOCE. To determine the extent of store depletion, a 10 mM caffeine bolus was perfused before the Ca^{2+}-containing Ringers was applied.

Involuntary running

The protocol for involuntary running was previously described (6). Briefly, 3-month-old mice were subjected to involuntary treadmill running (Omni-Pacer LC4/M; Columbus Instruments International) for 50 min or until exhaustion. The mice were given a 10 min acclimatization period at a speed of 6 m/min with the shock grid off and then the shock grid was activated and the speed was progressively increased by 2 m/min every 3 min until a maximum speed of 18 m/min was attained. The criterion for exhaustion was remaining on the shock grid for more than five consecutive seconds.

In situ isometric muscle force measurements

Mice were anesthetized with an intraperitoneal injection of a ketamine cocktail and maintained on isoflurane throughout the experiment. The distal tendon of the TA muscle was exposed and 4-0 nylon suture was tied at the muscle–tendon interface. The knee and foot of the mouse was secured to a platform and the tendon was mounted to a servomotor (Aurora Scientific). The TA muscle was stimulated using two intramuscular electrodes placed on either side of the peroneal nerve at 200 Hz. Stimulation voltages and optimal muscle length were adjusted to produce maximum isometric twitch force. A series of five consecutive tetanic isometric contractions were performed with a 2 min rest period between each contraction. Specific force was measured by dividing the active force by the muscle's physiologic cross-sectional area and the percent drop in force was determined by taking the difference in force between contractions 1 and 5.

Statistics

All results are presented as mean SEM. *P*-values <0.05 were considered significant and all assessment of significance was performed with a Student's *t*-test.

SUPPLEMENTARY MATERIAL

Supplementary Material is available at *HMG* online.

Conflict of Interest statement. None declared.

FUNDING

This work was supported by grants from the National Institutes of Health [to J.D.M., J.D. (1K99HL119353-01), and R.T.D. (AR059646)]. J.D.M. is also supported by the Howard Hughes Medical Institute. L.W.-L. was supported by the Academia Dei Lincea Fund and S.A.G. by the local affiliate of the American Heart Association.

REFERENCES

1. Rahimov, F. and Kunkel, L.M. (2013) The cell biology of disease: cellular and molecular mechanisms underlying muscular dystrophy. *J. Cell Biol.*, **201**, 499–510.
2. Kaplan, J.C. (2009) Gene table of monogenic neuromuscular disorders (nuclear genome only). *Neuromuscul. Disord.*, **19**, 77–98.
3. Millay, D.P., Goonasekera, S.A., Sargent, M.A., Maillet, M., Aronow, B.J. and Molkentin, J.D. (2009) Calcium influx is sufficient to induce muscular dystrophy through a TRPC-dependent mechanism. *Proc. Natl Acad. Sci. USA*, **106**, 19023–19028.
4. Whitehead, N.P., Yeung, E.W. and Allen, D.G. (2006) Muscle damage in mdx (dystrophic) mice: role of calcium and reactive oxygen species. *Clin. Exp. Pharmacol. Physiol.*, **33**, 657–662.
5. Spencer, M.J., Croall, D.E. and Tidball, J.G. (1995) Calpains are activated in necrotic fibers from mdx dystrophic mice. *J. Biol. Chem.*, **270**, 10909–10914.
6. Goonasekera, S.A., Lam, C.K., Millay, D.P., Sargent, M.A., Hajjar, R.J., Kranias, E.G. and Molkentin, J.D. (2011) Mitigation of muscular dystrophy in mice by SERCA overexpression in skeletal muscle. *J. Clin. Invest.*, **121**, 1044–1052.
7. Allen, D.G., Gervasio, O.L., Yeung, E.W. and Whitehead, N.P. (2010) Calcium and the damage pathways in muscular dystrophy. *Can. J. Physiol. Pharmacol.*, **88**, 83–91.
8. Hopf, F.W., Turner, P.R. and Steinhardt, R.A. (2007) Calcium misregulation and the pathogenesis of muscular dystrophy. *Subcell. Biochem.*, **45**, 429–464.
9. Badalamente, M.A. and Stracher, A. (2000) Delay of muscle degeneration and necrosis in mdx mice by calpain inhibition. *Muscle Nerve*, **23**, 106–111.
10. Fraysse, B., Nagi, S.M., Boher, B., Ragot, H., Laine, J., Salmon, A., Fiszman, M.Y., Toussaint, M. and Fromes, Y. (2010) Ca2+ overload and mitochondrial permeability transition pore activation in living delta-sarcoglycan-deficient cardiomyocytes. *Am. J. Physiol. Cell Physiol.*, **299**, C706–C713.
11. Millay, D.P., Sargent, M.A., Osinska, H., Baines, C.P., Barton, E.R., Vuagniaux, G., Sweeney, H.L., Robbins, J. and Molkentin, J.D. (2008) Genetic and pharmacologic inhibition of mitochondrial-dependent necrosis attenuates muscular dystrophy. *Nat. Med.*, **14**, 442–447.
12. Gailly, P. (2002) New aspects of calcium signaling in skeletal muscle cells: implications in Duchenne muscular dystrophy. *Biochim. Biophys. Acta*, **1600**, 38–44.
13. Edwards, J.N., Friedrich, O., Cully, T.R., von Wegner, F., Murphy, R.M. and Launikonis, B.S. (2010) Upregulation of store-operated Ca2+ entry in dystrophic mdx mouse muscle. *Am. J. Physiol. Cell Physiol.*, **299**, C42–C50.
14. Edwards, J.N., Murphy, R.M., Cully, T.R., von Wegner, F., Friedrich, O. and Launikonis, B.S. (2010) Ultra-rapid activation and deactivation of store-operated Ca(2+) entry in skeletal muscle. *Cell Calcium*, **47**, 458–467.
15. Lyfenko, A.D. and Dirksen, R.T. (2008) Differential dependence of store-operated and excitation-coupled Ca2+ entry in skeletal muscle on STIM1 and Orai1. *J. Physiol.*, **586**, 4815–4824.
16. Stiber, J.A. and Rosenberg, P.B. (2011) The role of store-operated calcium influx in skeletal muscle signaling. *Cell Calcium*, **49**, 341–349.
17. Yarotskyy, V. and Dirksen, R.T. (2012) Temperature and RyR1 regulate the activation rate of store-operated Ca(2)+ entry current in myotubes. *Biophys. J.*, **103**, 202–211.
18. Zhao, X., Moloughney, J.G., Zhang, S., Komazaki, S. and Weisleder, N. (2012) Orai1 mediates exacerbated Ca(2+) entry in dystrophic skeletal muscle. *PLoS ONE*, **7**, e49862.
19. Dirksen, R.T. (2009) Checking your SOCCs and feet: the molecular mechanisms of Ca2+ entry in skeletal muscle. *J. Physiol.*, **587**, 3139–3147.
20. Launikonis, B.S., Murphy, R.M. and Edwards, J.N. (2010) Toward the roles of store-operated Ca2+ entry in skeletal muscle. *Pflugers Arch.*, **460**, 813–823.
21. Li, T., Finch, E.A., Graham, V., Zhang, Z.S., Ding, J.D., Burch, J., Oh-hora, M. and Rosenberg, P. (2012) STIM1-Ca(2+) signaling is required for the hypertrophic growth of skeletal muscle in mice. *Mol. Cell Biol.*, **32**, 3009–3017.
22. Thornton, A.M., Zhao, X., Weisleder, N., Brotto, L.S., Bougoin, S., Nosek, T.M., Reid, M., Hardin, B., Pan, Z., Ma, J. *et al.* (2011) Store-operated Ca(2+) entry (SOCE) contributes to normal skeletal muscle contractility in young but not in aged skeletal muscle. *Aging (Albany NY)*, **3**, 621–634.
23. Stiber, J., Hawkins, A., Zhang, Z.S., Wang, S., Burch, J., Graham, V., Ward, C.C., Seth, M., Finch, E., Malouf, N. *et al.* (2008) STIM1 signalling controls store-operated calcium entry required for development and contractile function in skeletal muscle. *Nat. Cell Biol.*, **10**, 688–697.
24. Vig, M., DeHaven, W.I., Bird, G.S., Billingsley, J.M., Wang, H., Rao, P.E., Hutchings, A.B., Jouvin, M.H., Putney, J.W. and Kinet, J.P. (2008) Defective mast cell effector functions in mice lacking the CRACM1 pore subunit of store-operated calcium release-activated calcium channels. *Nat. Immunol.*, **9**, 89–96.
25. Kiviluoto, S., Decuypere, J.P., De Smedt, H., Missiaen, L., Parys, J.B. and Bultynck, G. (2011) STIM1 as a key regulator for Ca2+ homeostasis in skeletal-muscle development and function. *Skelet. Muscle*, **1**, 16.
26. Hoover, P.J. and Lewis, R.S. (2011) Stoichiometric requirements for trapping and gating of Ca2+ release-activated Ca2+ (CRAC) channels by stromal interaction molecule 1 (STIM1). *Proc. Natl Acad. Sci. USA*, **108**, 13299–13304.
27. Wei-Lapierre, L., Carrell, E.M., Boncompagni, S., Protasi, F. and Dirksen, R.T. (2013) Orai1-dependent calcium entry promotes skeletal muscle growth and limits fatigue. *Nat. Commun.*, **4**, 2805.
28. Cully, T.R., Edwards, J.N., Friedrich, O., Stephenson, D.G., Murphy, R.M. and Launikonis, B.S. (2012) Changes in plasma membrane Ca-ATPase and stromal interacting molecule 1 expression levels for Ca(2+) signaling in dystrophic mdx mouse muscle. *Am. J. Physiol. Cell Physiol.*, **303**, C567–C576.
29. Cahalan, M.D., Zhang, S.L., Yeromin, A.V., Ohlsen, K., Roos, J. and Stauderman, K.A. (2007) Molecular basis of the CRAC channel. *Cell Calcium*, **42**, 133–144.
30. Kim, M.S., Zeng, W., Yuan, J.P., Shin, D.M., Worley, P.F. and Muallem, S. (2009) Native store-operated Ca2+ influx requires the channel function of Orai1 and TRPC1. *J. Biol. Chem.*, **284**, 9733–9741.
31. Salido, G.M., Jardin, I. and Rosado, J.A. (2011) The TRPC ion channels: association with Orai1 and STIM1 proteins and participation in capacitative and non-capacitative calcium entry. *Adv. Exp. Med. Biol.*, **704**, 413–433.
32. Smyth, J.T., Dehaven, W.I., Jones, B.F., Mercer, J.C., Trebak, M., Vazquez, G. and Putney, J.W. Jr. (2006) Emerging perspectives in store-operated Ca2+ entry: roles of Orai, Stim and TRP. *Biochim. Biophys. Acta*, **1763**, 1147–1160.
33. Srikanth, S. and Gwack, Y. (2012) Orai1, STIM1, and their associating partners. *J. Physiol.*, **590**, 4169–4177.
34. Vaca, L. (2010) SOCIC: the store-operated calcium influx complex. *Cell Calcium*, **47**, 199–209.
35. Bernardi, P. and Rasola, A. (2007) Calcium and cell death: the mitochondrial connection. *Subcell Biochem.*, **45**, 481–506.
36. Duchen, M.R. (2000) Mitochondria and Ca(2+)in cell physiology and pathophysiology. *Cell Calcium*, **28**, 339–348.
37. Gwack, Y., Srikanth, S., Feske, S., Cruz-Guilloty, F., Oh-hora, M., Neems, D.S., Hogan, P.G. and Rao, A. (2007) Biochemical and functional characterization of Orai proteins. *J. Biol. Chem.*, **282**, 16232–16243.
38. Schneider, J.S., Shanmugam, M., Gonzalez, J.P., Lopez, H., Gordan, R., Fraidenraich, D. and Babu, G.J. (2013) Increased sarcolipin expression and decreased sarco(endo)plasmic reticulum Ca2+ uptake in skeletal muscles of mouse models of Duchenne muscular dystrophy. *J. Muscle Res. Cell Motil.*, **34**, 349–356.
39. Vandebrouck, C., Martin, D., Colson-Van Schoor, M., Debaix, H. and Gailly, P. (2002) Involvement of TRPC in the abnormal calcium influx observed in dystrophic (mdx) mouse skeletal muscle fibers. *J. Cell Biol.*, **158**, 1089–1096.
40. Wissing, E.R., Millay, D.P., Vuagniaux, G. and Molkentin, J.D. (2010) Debio-025 is more effective than prednisone in reducing muscular pathology in mdx mice. *Neuromuscul. Disord.*, **20**, 753–760.
41. Iwata, Y., Katanosaka, Y., Arai, Y., Shigekawa, M. and Wakabayashi, S. (2009) Dominant-negative inhibition of Ca2+ influx via TRPV2 ameliorates muscular dystrophy in animal models. *Hum. Mol. Genet.*, **18**, 824–834.
42. Whitehead, N.P., Streamer, M., Lusambili, L.I., Sachs, F. and Allen, D.G. (2006) Streptomycin reduces stretch-induced membrane permeability in muscles from mdx mice. *Neuromuscul. Disord.*, **16**, 845–854.
43. Cheng, K.T., Liu, X., Ong, H.L. and Ambudkar, I.S. (2008) Functional requirement for Orai1 in store-operated TRPC1-STIM1 channels. *J. Biol. Chem.*, **283**, 12935–12940.
44. Smyth, J.T., Hwang, S.Y., Tomita, T., DeHaven, W.I., Mercer, J.C. and Putney, J.W. (2010) Activation and regulation of store-operated calcium entry. *J. Cell Mol. Med.*, **14**, 2337–2349.
45. Bohm, J., Chevessier, F., Maues De Paula, A., Koch, C., Attarian, S., Feger, C., Hantai, D., Laforet, P., Ghorab, K., Vallat, J.M. *et al.* (2013) Constitutive

activation of the calcium sensor STIM1 causes tubular-aggregate myopathy. *Am. J. Hum. Genet.*, **92**, 271–278.
46. Darbellay, B., Arnaudeau, S., Bader, C.R., Konig, S. and Bernheim, L. (2011) STIM1L is a new actin-binding splice variant involved in fast repetitive Ca2+ release. *J. Cell Biol.*, **194**, 335–346.
47. Brennan, K.J. and Hardeman, E.C. (1993) Quantitative analysis of the human alpha-skeletal actin gene in transgenic mice. *J. Biol. Chem.*, **268**, 719–725.
48. Hack, A.A., Lam, M.Y., Cordier, L., Shoturma, D.I., Ly, C.T., Hadhazy, M.A., Hadhazy, M.R., Sweeney, H.L. and McNally, E.M. (2000) Differential requirement for individual sarcoglycans and dystrophin in the assembly and function of the dystrophin-glycoprotein complex. *J. Cell Sci.*, **113**(Pt 14), 2535–2544.
49. Wilkins, B.J., Dai, Y.S., Bueno, O.F., Parsons, S.A., Xu, J., Plank, D.M., Jones, F., Kimball, T.R. and Molkentin, J.D. (2004) Calcineurin/NFAT coupling participates in pathological, but not physiological, cardiac hypertrophy. *Circ. Res.*, **94**, 110–118.
50. Frezza, C., Cipolat, S. and Scorrano, L. (2007) Organelle isolation: functional mitochondria from mouse liver, muscle and cultured fibroblasts. *Nat. Protoc.*, **2**, 287–295.
51. Fewell, J.G., Osinska, H., Klevitsky, R., Ng, W., Sfyris, G., Bahrehmand, F. and Robbins, J. (1997) A treadmill exercise regimen for identifying cardiovascular phenotypes in transgenic mice. *Am. J. Physiol.*, **273**, H1595–H1605.
52. Parsons, S.A., Millay, D.P., Wilkins, B.J., Bueno, O.F., Tsika, G.L., Neilson, J.R., Liberatore, C.M., Yutzey, K.E., Crabtree, G.R., Tsika, R.W. *et al.* (2004) Genetic loss of calcineurin blocks mechanical overload-induced skeletal muscle fiber type switching but not hypertrophy. *J. Biol. Chem.*, **279**, 26192–26200.